Chiral and Achiral Contributions to Sum-Frequency Generation from Optically Active Solutions of Binaphthol†

P. Fischer,*,‡ F. W. Wise,§ and A. C. Albrecht‡

Department of Chemistry and Chemical Biology, and Department of Applied and Engineering Physics, Cornell University, Ithaca, New York 14853-1301

Received: December 30, 2002; In Final Form: April 19, 2003

The nonlinear sum- and difference-frequency generation spectroscopies can be probes of molecular chirality in optically active systems. We present a tensorial analysis of the chirality-specific electric-dipolar sum-frequency-generation susceptibility and the achiral electric-quadrupolar and magnetic-dipolar nonlinearities at second order in isotropic media. The chiral and achiral contributions to the sum-frequency signal from the bulk of optically active solutions of 1,1′-bi-2-naphthol (2,2′-dehydroxy-1,1′-binaphthyl) can be distinguished, and the former dominates. Ab initio computations reveal the dramatic resonance enhancement that the isotropic component of the electric-dipolar three-wave mixing hyperpolarizability experiences. Away from resonance its magnitude rapidly decreases, as—unlike the vector component—it is zero in the static limit. The dispersion of the first hyperpolarizability is computed by a configuration interaction singles sum-over-states approach with explicit regard to the Franck−Condon active vibrational substructure for all resonant electronic states.

1. Introduction

Chiro-optical methods are sensitive probes of molecular stereochemistry that can be applied to biological molecules in vivo. Conventional optical activity phenomena in linear optics include circular dichroism and optical rotation. Both measure the asymmetry in the response of an optically active medium to left and right circularly polarized light.[1] Electric-dipolar and the generally weaker magnetic-dipolar (and electric-quadrupolar) transitions underlie these effects; e.g., the rotational strength of the $j \leftarrow g$ transition is given by $\mathrm{Im}[\langle g|\vec{\mu}|j\rangle \cdot \langle j|\vec{m}|g\rangle]$.

In contrast, the nonlinear optical phenomena of second-harmonic generation (SHG), and sum- and difference-frequency generation (SFG, DFG) can give rise to nonlinear optical activity effects[2,3] and chirality specific signals[4−6] that arise in the electric dipole approximation. Intensity differences observed in nonlinear optical activity can therefore be larger by several orders of magnitude compared to analogous intensity differences in linear optical activity measurements.[3]

Third-order effects that probe chirality in isotropic media have also been reported;[7−9] however, they, similar to the linear optical effects, again require magnetic-dipolar transitions.

Near resonant electronic sum-frequency generation has recently been observed in solutions of chiral 1,1′-bi-2-naphthol (2,2′-dehydroxy-1,1′-binaphthyl, or BN) (see Figure 1) in tetrahydrofuran (THF).[5,6] The chiral specificity of these signals arises from the isotropic component of the electric-dipolar first hyperpolarizability, $\bar{\beta}$. This isotropic component, however, has no static limit and is even near resonance generally much weaker compared to a regular nonzero tensor component of the first hyperpolarizability.[10,11] We use ab initio sum-over-states computations to compute the relative dispersion of the isotropic and the vector component of the electric-dipolar sum-frequency-generation hyperpolarizability for chiral BN. For the experiments reported to date,[5,6] we calculate that the magnitude of $\bar{\beta}$ is at least 2−3 orders of magnitude smaller than the magnitude of the vector component of the first hyperpolarizability, $\beta_{\|}$. This leads us to consider higher order multipolar (and surface) contributions as potential sources of bulk sum- or difference-frequency generation. A tensorial analysis that explicitly separates the purely electric dipolar first hyperpolarizability from hyperpolarizabilities which include one magnetic- or electric-quadrupolar transition indicates that the chiral and achiral contributions to the total signal can be discerned based on their different polarization dependence.[6,12] Here we build on our recent work[6] and report complete polarization experiments for BN.

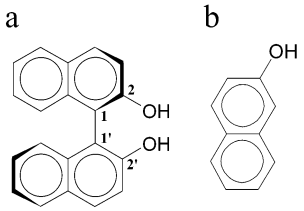

Figure 1. Structures of (a) R-(+)-1,1′-bi-2-naphthol and (b) 2-naphthol (2-hydroxynaphthalene, or 2HN).

The dispersion of the second-harmonic-generation hyperpolarizability for BN has been discussed by Byers et al., who consider only electronic spectral effects, but note the importance of vibronic features in the absorption spectrum of BN.[13] Recently Belkin et al. have developed a simple coupled oscillator model to describe the (electronic) sum-frequency response of BN for which they find good agreement with experiment.[14] Such a model is attractive as exciton delocalization in BN (C_2 geometry) can account for its chirality. However, the model requires large excitonic splittings that are not supported by quantum chemical computations. It also neglects vibrational structure, which is required to account for the linear absorption spectrum of the monomer of BN (see Figures 1 and 3), and which is thus

† Part of the special issue "A. C. Albrecht Memorial Issue".

* Corresponding author. E-mail: pf43@cornell.edu.
‡ Department of Chemistry and Chemical Biology.
§ Department of Applied and Engineering Physics.

10.1021/jp027861+ CCC: $25.00
Published on Web 06/26/2003

similarly important in the spectrum of BN itself.[13,15] Considering the evident importance of vibronic structure in the linear absorption spectrum of BN, we are compelled to include it in the description of its resonant nonlinear response. To this end we describe a general procedure that permits inclusion of vibrational substructures in the sum-over-states computation of the first hyperpolarizability. Application of such a procedure for BN leads us to conclude that the dispersion of the resonant sum-frequency signal indeed arises from Franck−Condon progressions of weakly split excitonic states.

2. Dispersion of $\bar{\beta}$ and $\beta_{\|}$ for BN

The Fourier component of the polarization at the sum frequency $P_\alpha^{(2)}(-\omega_3;\omega_1,\omega_2)$ induced by two incident fields, $E_\beta(\omega_1)$, and $E_\gamma(\omega_2)$, may in the electric dipole approximation (EDA) be written as

$$P_\alpha^{(2)}(-\omega_3;\omega_1,\omega_2) = \epsilon_0\, \chi_{\alpha\beta\gamma}^{(eee)} E_\beta(\omega_1)\, E_\gamma(\omega_2) + ... \qquad (1)$$

where $\omega_3 = \omega_1 + \omega_2$ and where (*eee*) labels the three electric dipole transition moments that appear in the expression for the corresponding hyperpolarizability (see eq 3). The scattering power at the sum frequency is related to $|P_\alpha^{(2)}|^2$. Higher order multipolar contributions to eq 1 are ignored in the EDA.

The electric-dipolar susceptibility $\chi_{\alpha\beta\gamma}^{(eee)}$ has only one independent nonvanishing component in an isotropic medium, the completely antisymmetric $\epsilon_{\alpha\beta\gamma}\, \chi^{(eee)}$. It in turn may be related to the first hyperpolarizability for each molecular species ξ, present with number density N_ξ:

$$\chi^{(eee)} = \sum_\xi \frac{N_\xi}{2\epsilon_0} \frac{1}{6} \epsilon_{\alpha\beta\gamma}\, \beta_{\xi,\alpha\beta\gamma}^{(eee)} = \sum_\xi \frac{N_\xi}{2\epsilon_0} \bar{\beta}$$

$$= \sum_\xi \frac{N_\xi}{12\epsilon_0} (\beta_{\xi,xyz}^{(eee)} - \beta_{\xi,xzy}^{(eee)} + \beta_{\xi,yzx}^{(eee)} - \beta_{\xi,yxz}^{(eee)} + \beta_{\xi,zxy}^{(eee)} - \beta_{\xi,zyx}^{(eee)}) \qquad (2)$$

where $\epsilon_{\alpha\beta\gamma}$ is the Levi−Civita tensor. For clarity we neglect local field factors. The pseudoscalar $\bar{\beta}$ is only nonzero for chiral molecules, as it vanishes for any molecule that possesses a center of inversion, a mirror plane, or a rotation-reflection axis. In Rayleigh−Schrödinger perturbation theory the sum-over-states expression for the first hyperpolarizability takes the form[16]

$$\beta_{\alpha\beta\gamma}^{(eee)}(-\omega_3;\omega_1,\omega_2) = \frac{1}{\hbar^2} P_I \sum_{k,g} \left\{ \frac{\mu_{\mathbf{gk}_\alpha} \bar{\mu}_{kj_\beta} \mu_{jg_\gamma}}{(\tilde{\omega}_{kg} - \omega_3)(\tilde{\omega}_{jg} - \omega_2)} + \frac{\mu_{gk_\beta} \bar{\mu}_{kj_\alpha} \mu_{jg_\gamma}}{(\tilde{\omega}_{kg}^* + \omega_1)(\tilde{\omega}_{jg} - \omega_2)} + \frac{\mu_{gk_\beta} \bar{\mu}_{kj_\gamma} \mu_{jg_\alpha}}{(\tilde{\omega}_{kg}^* + \omega_1)(\tilde{\omega}_{jg}^* + \omega_3)} \right\} \qquad (3)$$

where the summation is over all intermediate states *k*, *j*, and where P_I is a permutation operator that simultaneously permutes the incident optical frequencies and their associated Cartesian coordinates (ω_1, β), and (ω_2, γ). The α component of the transition electric dipole moment $\langle g|\hat{\mu}_\alpha|k\rangle$, is written as μ_{gk_α}, and $\bar{\boldsymbol{\mu}}$ is the fluctuation dipole operator $\bar{\boldsymbol{\mu}} = \hat{\boldsymbol{\mu}} - \langle g|\hat{\boldsymbol{\mu}}\,|g\rangle$.[17] By defining the transition frequency to be the complex quantity $\tilde{\omega}_{kg} = \omega_{kg} - i\Gamma_{kg}$, where ω_{kg} is the real transition frequency and Γ_{kg} is half the width at half the maximum height of the transition from the ground state *g* to the upper level *k*, eq 3 may be used near resonance. In Rayleigh−Schrödinger perturbation theory the isotropic component of the first electric-dipolar hyperpolarizability for sum-frequency generation may be written as

$$\bar{\beta}(-\omega_3;\omega_1,\omega_2) = \frac{(\omega_2 - \omega_1)}{\hbar^2} \frac{1}{6} \epsilon_{\alpha\beta\gamma} \mu_{gk_\alpha} \bar{\mu}_{kj_\beta} \mu_{jg_\gamma} \times \left\{ \frac{1}{(\tilde{\omega}_{jk} - \omega_3)(\tilde{\omega}_{jg} - \omega_2)(\tilde{\omega}_{jg} - \omega_1)} + \frac{1}{(\tilde{\omega}_{kj}^* + \omega_3)(\tilde{\omega}_{kg}^* + \omega_2)(\tilde{\omega}_{kg}^* + \omega_1)} + \frac{1}{(\tilde{\omega}_{kg} - \omega_3)(\tilde{\omega}_{jg} - \omega_2)(\tilde{\omega}_{jg} - \omega_1)} \right\} + \frac{1}{(\tilde{\omega}_{jg}^* + \omega_3)(\tilde{\omega}_{kg}^* + \omega_2)(\tilde{\omega}_{kg}^* + \omega_1)} \qquad (4)$$

We also define a vector component of the first hyperpolarizability in the direction of the permanent dipole moment $\mu_\alpha^{(0)}$

$$\beta_{\|} = \frac{3}{5} \frac{\mu_\alpha^{(0)} \beta_{\alpha\beta\beta}^{(eee)}}{(\mu_\gamma^{(0)}\, \mu_\gamma^{(0)})^{1/2}} \qquad (5)$$

as an approximate measure for the strength of the hyperpolarizability components that are likely to be probed by hyper-Rayleigh scattering, electric-field-induced three-wave mixing, or second-order nonlinear optical surface experiments. Summation over repeated indices is implied.

To estimate the relative strength of the chirality-specific sum-frequency-generation nonlinearity $\bar{\beta}$, we compute its dispersion and compare it to that of $\beta_{\|}$.

The C_2 geometry of BN (see Figure 1) is fully optimized in a restricted Hartree−Fock computation with the correlation consistent polarized valence double-ζ (cc-pVDZ) basis[18] in Gaussian98.[19] Since we are interested in the dispersion of the electric-dipolar first hyperpolarizabilty including near resonance, we use a configuration interaction singles sum-over-states (CIS-SOS) procedure to compute the tensor components of the first hyperpolarizability in eq 3. The first 80 excited states (singlets), their electric dipole transition moments to the ground state, and the excited state dipoles are computed at the CIS/cc-pVDZ level of approximation in Gaussian98.[19] For now we do not explicitly consider vibrational substructure of the electronic transitions; rather we assume that it can be subsumed by relatively large phenomenological line-widths (taken to be 1500 cm^{-1} hwhm for all transitions). We find that even when accounting for the absence of vibronic features in the computations, the CIS calculations do not reproduce the features of BN's linear absorption spectrum well. In particular, the lowest excited state is not captured by the CIS/cc-pVDZ computations and the energy spacing of the computed excited states is only in fair agreement with the experimental UV−vis spectrum. Similar results were obtained for the 631+G(d), 631+G(d,p), and 6311+G(d,p) basis sets. The CIS results suggest that higher substitutions ought to be included in the configuration interaction. Due to the considerable increase in computational cost such calculations would require, we nevertheless proceed with the CIS results and reduce all excitation energies by 1.436 eV such that the first computed excited state (weak excitonically split singlet) comes into register with the experimentally observed

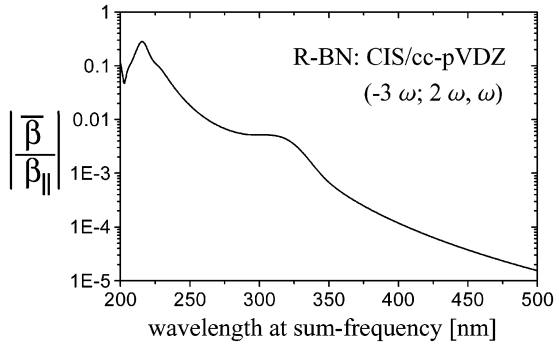

Figure 2. Dispersion of the isotropic and vector components of the first electric-dipolar sum-frequency generation ($3\omega = 2\omega + \omega$) hyperpolarizability for chiral BN.

absorption at 336 nm. This ensures that the computed excitonic states with $f \approx 1.8$ lie within ~10 nm of the experimentally observed absorption peak at 228 nm. We find that the ab inito CIS-SOS/cc-pVDZ computed magnitude of $\bar{\beta}$ at 266 nm and at 345 nm agrees within a factor of ~2 with the experimentally reported strengths of $\bar{\beta}$ for BN[5,6] (vide infra). Also, the CIS-SOS/cc-pVDZ second-harmonic generation $\beta_{zzz}^{(eee)}$ at 532 nm for BN is, as one would expect, somewhat weaker (about half the strength of the weakest $\beta_{zzz}^{(eee)}$) ($z \parallel C_2$) than those of 6,6′-disubstituted binaphthols measured by hyper-Rayleigh scattering.[20]

Figure 2 shows the dispersion of $|\bar{\beta}/\beta_{\parallel}|$ from a CIS-SOS /cc-pVDZ computation for R-(+)-1,1′-bi-2-naphthol. It is possible that by considering the ratio of $\bar{\beta}/\beta_{\parallel}$ there is some cancellation of errors, although the shape of the respective dispersion curves is unlikely to be correct on resonance for the aforementioned reasons plus the neglect of vibrational structure. It is seen that the resonance enhancement of the chiral property tensor $\bar{\beta}$ is much more dramatic than that of the achiral $\beta_{\parallel}$, or indeed any other tensor component, as unlike $\beta_{\parallel}$, $\bar{\beta} = 0$ in the static limit (degenerate incident frequencies).[21,22] Due to the absence of any diagonal contributions to the sum-over-states in eq 4, the magnitude of the pseudoscalar hyperpolarizability and hence $\bar{\beta}/\beta_{\parallel}$ is small (away from resonance) even when the chiral molecules are highly conjugated such as in the case of helicenes.[23]

Given the overall weakness of $|\bar{\beta}/\beta_{\parallel}|$, it may thus be important to consider, in addition to the chirality-specific electric-dipolar three-wave mixing hyperpolarizability from the optically active bulk, other potential sum-frequency (and difference-frequency) generators, such as magnetic-dipolar and electric-quadrupolar bulk nonlinearities and electric-dipolar surface nonlinearities. A tensorial analysis of such generators is presented in section 4.

First, however, we describe a simple, general procedure to incorporate vibrational substructure in electronic SOS computations to better describe the dispersion of $\bar{\beta}$ near resonance.

3. Modeling Franck−Condon Vibrational Substructure in Calculations of $\bar{\beta}$

One quantum chemical approach in the calculation of the dynamic nonlinear optical response is to generate an electronic basis set with eigenenergies and a transition moment matrix to then perform the appropriate sum-over-states using Lorentzian poles. The widths are often chosen such that they reasonably account for typical bandwidths of electronic transitions, even though the widths are (in general) primarily due to Franck−Condon (F−C) vibrational substructure, and not due to homogeneous broadening. This approach (taken in section 2) may be acceptable for virtual transitions; however, when dealing with resonant or near resonant transitions,[24] as is the case in the SFG experiments on BN reported to date,[5,6] it is important to incorporate the vibronic structure.

In the following we shall elaborate the vibrational substructure for two electronic states, *a* and *b*, which are to be candidates for the "two state" resonances (or near resonant transitions) that are featured in the $\bar{\beta}$ calculations.[21] The treatment is readily extended to include more than two resonant states.

The major contribution to $\bar{\beta}$ in sum-frequency generation of these two states is a one-photon resonance (or near resonance) with state *a* (the lower lying state) and a two-photon resonance with state *b*. The transition moments involved for their contribution in the second-order polarization are, according to eq 4, $\vec{\mu}_{ag}$, $\vec{\mu}_{ab}$, and $\vec{\mu}_{bg}$. The experimental (vibronic) absorption bands from the ground state into the *a* and the *b* states relate directly to $|\vec{\mu}_{ag}|^2$ and $|\vec{\mu}_{bg}|^2$. In general, little is known about the $b \leftarrow a$ transition and certainly not its F−C vibrational substructure. Nevertheless, as we shall see, we can devise a procedure to reasonably model the vibrational substructure (and band shape) of this unknown transition, given the abundant experimental details concerning the $a \leftarrow g$ and $b \leftarrow g$ transitions.

We proceed first to decompose the structure of the two main transitions originating in the ground state as a sum of Lorentzians. The vibronic states shall now explicitly become members of the basis set (spawned from electronic states *a* and *b*) in the computation of $\bar{\beta}$. The remaining members of the basis set are to be treated as before. The transition moments for the individual Lorentzian components may be extracted from the fits and the computations, as, to a good approximation (negligible Herzberg−Teller coupling), we can assume that the vibronic substructure changes neither the direction nor the inherent magnitude of the transition moments. The peak positions, line-widths (from their best fits), and transition moments for all of the F−C vibrational substates related to electronic states *a* and *b*, as regards their link to the ground state, are now known. The $b \leftarrow a$ transition is, however, still undetermined.

We propose that a standard linear one-dimensional displaced harmonic oscillator model is applied for the F−C vibrational substructure of the best fit normalized band shapes $B_{a\leftarrow g}(\omega)$ and $B_{b\leftarrow g}(\omega)$. If one assumes a constant vibrational frequency for the principal F−C active mode, then the model generates one dimensionless displacement parameter for each of the two transitions, S_a and S_b. They represent the displacements of the excited state potential energy curves along the F−C active normal mode relative to the potential curve in the ground electronic state.[25] Now the unknown band for the $b \leftarrow a$ transition could be constructed if one knew the relative displacement of the potential curves for *a* and for *b*. The simple model would state that the relative displacement is just $|S_b - S_a|$. One can then construct a $B_{b\leftarrow a}(\omega)$ band, given appropriate considerations to the bandwidths of the Lorentzian components (these will follow from those fixed in the two reference bands). Since $\vec{\mu}_{ab}$ is available from quantum chemical computations, one then proceeds as above to recover all necessary components for a calculation of $\bar{\beta}$ in which two resonant (or near resonant) *a* and *b* states have their vibrational substructure broken out.

The lowest "two" states (really four given the excitonic splitting) of BN are obvious *a*, *b* candidates for such a study.

Application to 1,1′-Bi-2-naphthol. Structural studies of 1,1′-bi-2-naphthol predict that the planes of the 2-naphthol (2HN) groups (see Figure 1) are quasi-orthogonal (with dihedral angles of ±90° to ±100°).[15,26,27] Our quantum chemical computations

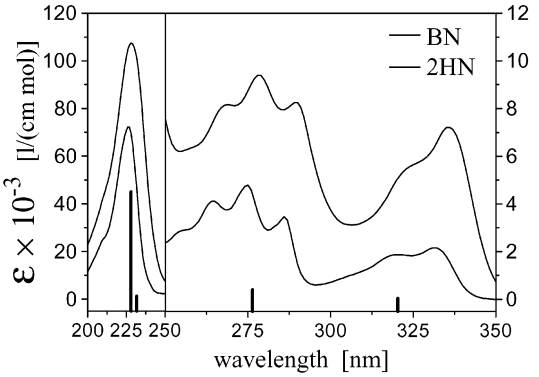

Figure 3. UV−vis spectra for BN (upper curve) and 2HN (lower curve) in ethanol obtained at ≈0.1 mM concentrations. Similar spectra were obtained in THF. The vertical lines represent the relative (ZINDO) oscillator strengths of the first four excited singlet states of 2HN (arbitrary units).

(in vacuo) approximately agree with these findings. Hartree−Fock calculations with the basis sets from section 2 find a dihedral angle $-89° < \theta(2-1-1'-2') < -86°$ for the R-enantiomer, and $\theta \approx -85°$ in computations with the semi-empirical AM1 Hamiltonian. This suggests that there is likely to be only weak coupling between the two naphthol rings. A comparison of the UV−vis absorption spectra for 2HN and BN, seen in Figure 3, shows that the absorption spectrum of BN indeed resembles that of 2HN. We, however, note that the BN solutions in the actual SFG experiments (this work and refs 5 and 6) are highly concentrated (∼0.5 M) and that this may give rise to perturbations not seen in the linear absorption spectrum or captured by the quantum chemical computations. We nevertheless proceed by analyzing these experiments by computations on isolated molecules. The subsequently obtained results warrant this approach.

The ZINDO procedure has been used to accurately model spectroscopic properties of organic π-electron chromophores and the ZINDO-SOS method to compute their nonlinear response.[28] For an AM1 optimized geometry of 2HN, a ZINDO computation in Gaussian98[19] locates the first four excited singlet states at 320 nm (with $f = 0.012$), at 276 nm ($f = 0.152$), at 232 nm ($f = 0.045$), and at 228 nm ($f = 1.72$), respectively (see also Pariser−Parr−Pople calculations by Hanazaki and Akimoto[15]). Accounting for solvatochromic shifts, these transitions may then be associated with the three bands observed in the absorption spectrum of 2HN in Figure 3. Franck−Condon progressions are clearly observed in the absorption spectrum of 2HN, and are thus expected to play an equally important role in the absorption spectrum of BN. The observed splitting of the lowest lying band of 2HN and BN is ≈1100 cm^{-1}.

Additional complexity arises in the spectrum of BN due to excitonic splitting of the excited states.[13,15] For example, the lowest two singlet states of BN are split by 136 cm^{-1} with $\theta = -85$ ($f = 0.055$ and 0.006) in a ZINDO-1 (AM1) computation (and 183 cm^{-1} for AM1/ZINDO-S). With $\theta(2-1-1'-2') = -100°$ the computed splitting approximately doubles, and at $-120°$ it is 474 cm^{-1}. Pariser−Parr−Pople SCF-CI calculations by Hanazaki et al. find a splitting of 560 cm^{-1} with $\theta = -100$ ($f = 0.054$ and 0.009),[15] whereas Hicks and co-workers compute an energy difference of 1129 cm^{-1} ($f = 0.055$ and 0.006) for the same dihedral angle. Such a splitting approaches the separation of the peaks observed in the absorption spectrum, but in the absence of F−C structure the observed relative peak intensities are not accounted for.

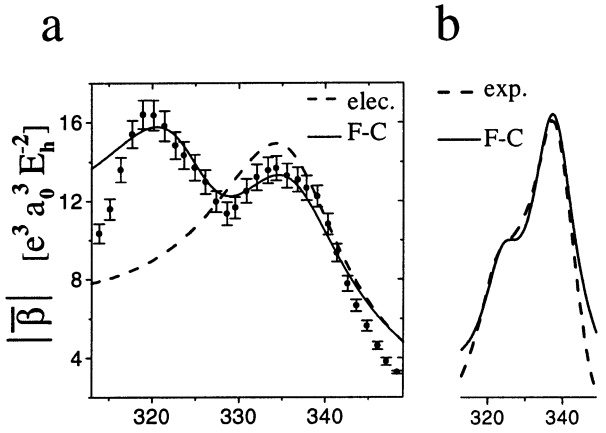

Figure 4. (a) Sum-frequency $\bar{\beta}$ in atomic units.[41] Solid dots are from ref 14 for sum-frequency generation from BN with one laser color fixed at 1059 nm. The solid lines correspond to scaled ZINDO-SOS (100 states) computations with the inclusion of F−C structure for the first exciton-split excited state (black line) and without the inclusion of vibrational structure (dashed line). All ZINDO $\bar{\beta}$ results are scaled such that they agree with off-resonant $\bar{\beta}$ CIS-SOS/cc-pVDZ computations which are believed to be more accurate far from resonance. In addition, the theoretical curves have been scaled by a factor of ∼2 to follow more closely the experimentally observed data. (b) A region of the UV−vis absorption spectrum of BN (dashed line) and a F−C simulation (black line) thereof.

Electronic structure calculations can in principle generate the electronic excited states and their splittings; the vibrational substructure of the bands, however, needs to be included separately. Tentative vibrational assignments have been reported for 2HN and BN.[29,30] We proceed by considering the simplest possible spectral simulation for BN by assuming only the presence of one F−C active normal mode with fixed vibrational frequency and line-width. From the absorption spectrum we obtain a displacement parameter ($S_a = 0.9$), the vibrational energy ($\nu_a = 1250$ cm^{-1}), and line-width (590 cm^{-1}), and use these to model the band shape in BN, where we take the splitting of the first exciton pair to be 350 cm^{-1} (approximate average of the computations including those of ref 15). For simplicity the F−C progression is truncated after inclusion of the first four terms. Improved band shapes and closer agreement with experiment away from the peaks for the linear and nonlinear response (vide infra) would be obtained by considering all F−C active normal modes with all terms in the F−C progression and by considering a convolution with a Gaussian distribution function to account for inhomogeneous broadening.[24] Extension to a density matrix analysis would in addition allow the description of pure-dephasing-induced resonances[21] and doubly resonant SFG. Nevertheless, our minimal F−C treatment approximately describes the absorption band shape in BN, as is seen in Figure 4b.

Together with a similar F−C analysis for the higher lying states of BN, we could proceed to model all observed band shapes to then explicitly include the (resonant) vibronic states in the basis for the SOS calculation as described in section 3. However, the sum-frequency dispersion reported by Belkin et al.[5,14] is only two-photon resonant with the lowest band and no intermediate resonances occur. We therefore only include vibrational F−C structure for the lowest exciton-split states in the calculation of $\bar{\beta}$. It is seen that the main features of the experimentally observed spectrum are captured by this simple model without recourse to large excitonic splittings (see Figure 4a). The purely Lorentzian line-shape analysis causes the theoretical curves in Figure 4 to be wider away from the peaks compared with the experimentally observed line shapes. The

approximate treatment of both the higher lying states and the F−C series also contributes to deviation of the computed dispersion of $\bar{\beta}$ from the experimental data (especially at shorter wavelengths). Despite these differences, we conclude that due to Franck−Condon progressions even small excitonic splittings (<400 cm^{-1}) that fully concur with quantum chemical computations can give rise to the observed doublet with much wider peak spacing. In contrast, the coupled oscillator analysis which ignores F−C structure uses a splitting of 1750 cm^{-1} for the lowest singlet state of BN.[14]

The inclusion of vibrational substructure has altered the shape of the computed dispersion for $\bar{\beta}$ near resonance; however, its strength relative to that of $\beta_{||}$, as shown in Figure 2, is largely unchanged. We therefore discuss whether higher order multipolar contributions could potentially mask any signals that are due to the chirality-specific $\bar{\beta}$. It has been reported that certain beam polarizations allow the achiral multipolar contributions to be separated from the chiral electric-dipolar signals.[5,6] Here we present a tensorial analysis of the multipolar bulk contributions for an isotropic medium and report a series of polarization experiments for BN.

4. Multipolar Contributions to Bulk Sum- and Difference-Frequency Generation

4.1. Tensorial Analysis. In eq 1 we consider only the electric-dipolar contribution to the induced nonlinear polarization that gives rise to sum-frequency generation. If, however, magnetic-dipolar and electric-quadrupolar terms are included, the total induced polarization at second order takes the form

$$P_\alpha^{(2,\mathrm{tot})} = P_\alpha^{(2)} + \frac{\mathrm{i}}{\omega_3}\epsilon_{\alpha\beta\gamma}\nabla_\beta M_\gamma - \nabla_\beta Q_{\beta\alpha} \tag{6}$$

where M_γ is the magnetization and $Q_{\beta\alpha}$ is the electric quadrupole moment per unit volume.

We consider electric-dipolar contributions and the lowest order correction to the EDA, where one of the field actions is taken beyond the electric dipole approximation, to include the gradient of the electric field $\nabla_\gamma E_\delta$ or a magnetic field action B_α. Consequently, one of the electric-dipolar (e) transition moments becomes either a magnetic-dipolar (m) transition moment or an electric-quadrupolar (Q) transition moment in the susceptibility that is taken beyond the EDA:[31]

$$\begin{aligned} P_\alpha^{(2)}(-\omega_3;\omega_1,\omega_2)/\epsilon_0 = {} & \chi_{\alpha\beta\gamma}^{(eee)}E_\beta(\omega_1)\,E_\gamma(\omega_2) \\ & + \chi_{\alpha\beta\gamma}^{(eme)}B_\beta(\omega_1)\,E_\gamma(\omega_2) \\ & + \chi_{\alpha\beta\gamma}^{(eem)}E_\beta(\omega_1)\,B_\gamma(\omega_2) + \chi_{\alpha\beta\gamma\delta}^{(eQe)}\nabla_\beta E_\gamma(\omega_1)\,E_\delta(\omega_2) \\ & + \chi_{\alpha\beta\gamma\delta}^{(eeQ)}E_\beta(\omega_1)\,\nabla_\gamma E_\delta(\omega_2) \end{aligned} \tag{7}$$

$$M_\alpha(-\omega_3;\omega_1,\omega_2)/\epsilon_0 = \chi_{\alpha\beta\gamma}^{(mee)}E_\beta(\omega_1)\,E_\gamma(\omega_2) \tag{8}$$

$$Q_{\beta\alpha}(-\omega_3;\omega_1,\omega_2)/\epsilon_0 = \chi_{\alpha\beta\gamma\delta}^{(Qee)}E_\gamma(\omega_1)\,E_\delta(\omega_2) \tag{9}$$

As in the case of the electric-dipolar susceptibility in eq 2, we are interested in the isotropic components[32] of the susceptibilities in eqs 7−9. We assume transverse waves and obtain

$$\begin{aligned} P_\alpha^{(2,\mathrm{tot})}(-\omega_3;\omega_1,\omega_2)/\epsilon_0 = {} & \epsilon_{\alpha\beta\gamma\chi}^{(eee)}E_\beta(\omega_1)\,E_\gamma(\omega_2) \\ & + \left\{\delta_{\alpha\gamma}\delta_{\beta\delta}\left(\frac{1}{\omega_3}\chi^{(eem)} + \mathrm{i}\chi_2^{(eeQ)}\right)\right. \\ & \left. + \delta_{\alpha\delta}\delta_{\beta\gamma}\left(\frac{-1}{\omega_3}\chi^{(eem)} + \mathrm{i}\chi_3^{(eeQ)}\right)\right\}E_\beta(\omega_1)\,k_\gamma(\omega_2)\,E_\delta(\omega_2) \\ & + \left\{\delta_{\alpha\beta}\delta_{\delta\gamma}\left(\frac{1}{\omega_3}\chi^{(eme)} + \mathrm{i}\chi_1^{(eQe)}\right)\right. \\ & \left. + \delta_{\alpha\gamma}\delta_{\beta\delta}\left(\frac{-1}{\omega_3}\chi^{(eme)} + \mathrm{i}\chi_2^{(eQe)}\right)\right\}k_\beta(\omega_1)\,E_\gamma(\omega_1)\,E_\delta(\omega_2) \\ & + \left\{\delta_{\alpha\gamma}\delta_{\beta\delta}\left(\frac{-1}{\omega_3}\chi^{(mee)} - \mathrm{i}\chi_3^{(Qee)}\right)\right. \\ & \left. + \delta_{\alpha\delta}\delta_{\beta\gamma}\left(\frac{1}{\omega_3}\chi^{(mee)} - \mathrm{i}\chi_2^{(Qee)}\right)\right\}k_\beta(\omega_3)\,E_\gamma(\omega_1)\,E_\delta(\omega_2) \end{aligned} \tag{10}$$

The wave vectors k_α change sign under time reversal, and thus the imaginary part of the $\chi^{(mee)}$ susceptibilities and the real part of the $\chi_i^{(Qee)}$ tensors ensure that the material response is even under time-reversal symmetry, as is required in the absence of a static magnetic field.[31,33] The magnetic-dipolar and electric-quadrupolar terms arise in pairs and can thus be combined into a single effective susceptibility.[31] The separate enumeration of terms in eq 10 should, however, be more amenable to quantum chemical computations. Selected resonances may also enable the isolation of either specific electric-quadrupolar or magnetic-dipolar contributions.[34]

The isotropic components in eq 10 are related to the molecular hyperpolarizabilities by

$$\chi^{(eem)} = \frac{N}{2\epsilon_0}\frac{1}{6}\beta_{\alpha\beta\gamma}^{(eem)}\epsilon_{\alpha\beta\gamma} \tag{11}$$

$$\chi_1^{(eeQ)} = \frac{N}{2\epsilon_0}\frac{1}{30}\left[4\beta_{\alpha\alpha\beta\beta}^{(eeQ)} - \beta_{\alpha\beta\alpha\beta}^{(eeQ)} - \beta_{\alpha\beta\beta\alpha}^{(eeQ)}\right] \tag{12}$$

$$\chi_2^{(eeQ)} = \frac{N}{2\epsilon_0}\frac{1}{30}\left[-\beta_{\alpha\alpha\beta\beta}^{(eeQ)} + 4\beta_{\alpha\beta\alpha\beta}^{(eeQ)} - \beta_{\alpha\beta\beta\alpha}^{(eeQ)}\right] \tag{13}$$

$$\chi_3^{(eeQ)} = \frac{N}{2\epsilon_0}\frac{1}{30}\left[-\beta_{\alpha\alpha\beta\beta}^{(eeQ)} - \beta_{\alpha\beta\alpha\beta}^{(eeQ)} + 4\beta_{\alpha\beta\beta\alpha}^{(eeQ)}\right] \tag{14}$$

and respective permutations for tensors with (*mee*), (*eme*), (*Qee*), and (*eQe*) (also note ref 35). The quantum mechanical expressions for the multipolar hyperpolarizabilities resemble the electric-dipolar hyperpolarizability (see eq 3) where one transition electric dipole moment is replaced by a transition magnetic dipole or a transition electric quadrupole moment.[36,37] These expressions can be used to compute the sum-over-states for multipolar hyperpolarizabilities.

As is seen in eq 10, it is not possible to distinguish between magnetic-dipolar and electric-quadrupolar contributions. However, the chirality-specific $\chi^{(eee)}$ is probed by polarization combinations different from those that access the susceptibilities which are taken beyond the EDA (and different from those that probe electric-dipolar susceptibilities which originate from the anisotropy at the cuvette/liquid interface). Thus chiral and achiral contributions to the signal may be distinguished, and bulk sum- and difference-frequency generation are essentially background-free probes of molecular chirality.

4.2. Polarization Experiments for SFG from BN. The polarization dependence of the chiral and achiral three-wave mixing susceptibilities follows from eq 10. The electric-dipolar $\chi^{(eee)}$ is multiplied by a Levi−Civita tensor and is thus probed

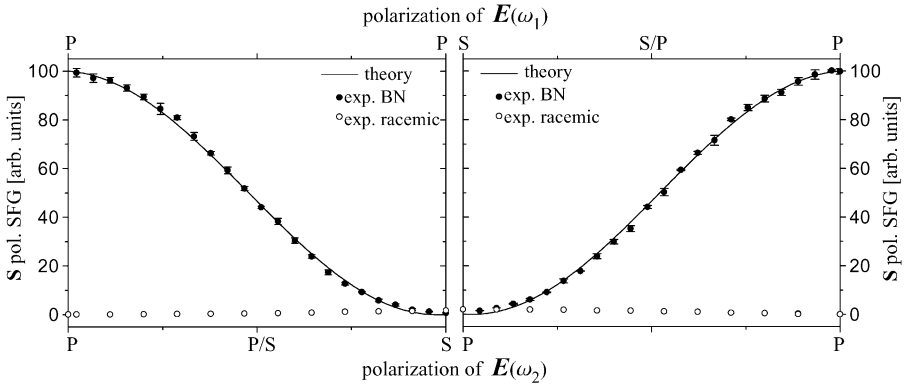

Figure 5. S-polarized SFG ($3\omega = 2\omega + \omega$) observed at 266 nm from chiral BN in THF (solid dots). The input polarizations are varied as indicated. The solid line is a fit from theory assuming only the presence of the electric-dipolar chirality-specific nonlinearity. Open circles correspond to measurements from a racemic solution of BN in THF measured at the same concentration.

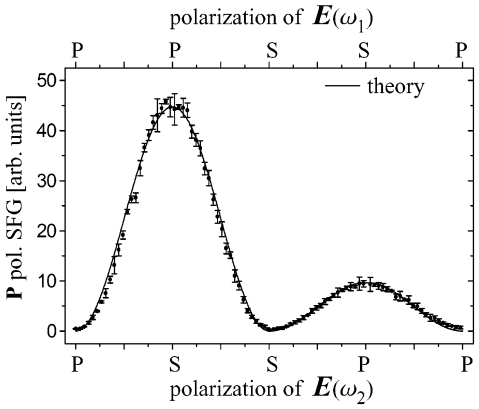

Figure 6. P-polarized SFG ($3\omega = 2\omega + \omega$) observed at 266 nm from chiral BN in THF (solid dots). The input polarizations are independently varied in 4° increments from P to S to P. The solid line is a fit from theory assuming only the presence of the electric-dipolar chirality-specific nonlinearity.

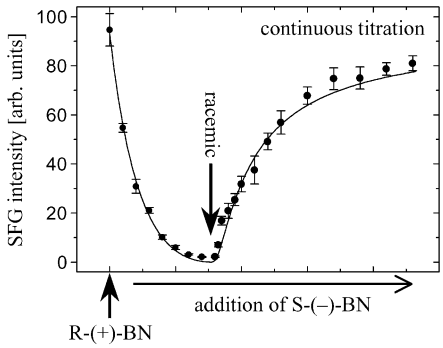

Figure 7. Titration starting with 0.5 M R-(+)-1,1′-bi-2-naphthol in THF to which S-(−)-1,1′-bi-2-naphthol (0.5 M in THF) is added until the solution becomes racemic. At this point some of the racemic solution is removed, and more S-(−)-1,1′-bi-2-naphthol (0.5 M in THF) is added. The electric-dipolar SFG is proportional to the square of the concentration difference of the two enantiomers, $([R] - [S])^2$, which is plotted by the solid line.

in a noncollinear beam geometry by the combination of one S- and two P-polarized waves (PPS, PSP, or SPP), whereas the Kronecker δ's that multiply the multipolar achiral bulk susceptibilities require that for transverse waves either all fields are P-polarized or that two fields are S-polarized and one is P-polarized (PPP, PSS, SPS, or SSP).

To observe SFG from the optically active bulk, $\bar{\beta}$ needs to be near resonance (vide supra), and in second-order processes this invariably means that the resonant wave(s) also experience linear absorption. Phase matching is absent in normally dispersive isotropic media and absorption will further reduce the coherence length (typically $<1\ \mu$m), such that contributions from the liquid/cuvette interface ($\sim\beta_{||}$) may become important. The molecular arrangement at the interface between two isotropic media is expected to be symmetric about the surface normal, and is then probed by the same polarization combinations (PPP, PSS, SPS, or SSP) that access the achiral bulk contributions.[38] Multipolar contributions have been observed in surface nonlinear optical activity experiments, and their susceptibilities have been found to be comparable to chiral electric-dipolar susceptibilities.[39,40] An all S-polarized field combination is a measure of the experimental "noise".

In Figures 5 and 6 we report SFG experiments at 266 nm from solutions of BN in THF where the polarization of all three waves is controlled. The polarization of the sum-frequency signal is fixed (either S in Figure 5 or P in Figure 6) and the polarization of the input waves is independently rotated. All experimental data points have been shifted by $\sim 2°$ to correct for a systematic offset in the experiments. Signal strengths for all measurements are relative to those measured with S-polarized signal and P-polarized incident waves. The solid lines in the figures show a prediction of the signal's polarization dependence from theory that assumes only the presence of the chirality-specific electric-dipolar nonlinearity $\chi^{(eee)}$. The data points closely follow the fits and the dominant contribution to the observed SFG hence stems from the electric-dipolar bulk nonlinearity, as is expected near resonance for BN. Our experiments are at the fixed harmonics of a Ti:sapphire laser (800, 400, and 266 nm) and we measure similar signal strengths for chiral 1,1′-bi-2-naphthol and 1,1′-binaphthyl-2,2′-diyl hydrogenphosphate solutions.

Further away from resonance the achiral bulk contributions are likely to become relatively more important. The chiral origin of the signal can be independently established by a titration as shown in Figure 7. Small deviations from the theoretical fits that assume only the presence of an electric-dipolar bulk response are nevertheless observed. In particular, the S-polarized signals from S- and P-polarized input beams in (Figure 5) are >0 and are comparable to those observed from a racemic mixture of BN. These achiral signals are above the noise level and have their origin either in electric-dipolar surface nonlinearities or arise from the magnetic-dipolar/electric-quadrupolar bulk susceptibilities. Should one of the beams have a mixed polarization, then the signal is sensitive to both the chiral and achiral contributions plus interference terms.[12]

5. Conclusions

We discuss the tensorial properties of electric-dipolar and higher order multipolar (beyond the electric dipole approximation) nonlinearities in isotropic media. The former may give rise to background-free signals that depend on the solution being optically active, whereas the latter exist for all media. Certain polarization combinations allow the two to be distinguished. This is demonstrated for sum-frequency-generation experiments from optically active solutions of 1,1′-bi-2-naphthol in tetrahydrofuran.

Quantum chemical CIS-SOS/cc-pVDZ computations of the dispersion of the vector relative to the (much weaker) isotropic component of the (electric-dipolar) sum-frequency-generation hyperpolarizability are reported.

We describe a general methodology that permits the inclusion of Franck−Condon vibrational substructure of (near) resonant electronic transitions in sum-over-states computations of $\vec{\beta}$. Application is made to two-photon-resonant sum-frequency generation from chiral 1,1′-bi-2-naphthol. Inclusion of vibronic effects are found to be necessary to accurately model the resonant sum-frequency response of BN.

Acknowledgment. P.F. is grateful to Professor A. D. Buckingham for many helpful discussions. Aid through grants from the NSF (CHE-0095056) and NIH (RR10075) as well as a NATO postdoctoral fellowship for P.F. are gratefully acknowledged.

References and Notes

(1) Barron, L. D. *Molecular Light Scattering and Optical Activity*; CUP: Cambridge, 1982.
(2) Petralli-Mallow, T.; Wong, T. M.; Byers, J. D.; Yee, H. I.; Hicks, J. M. *J. Phys. Chem.* **1993**, *97*, 1383.
(3) Byers, J. D.; Yee, H. I.; Hicks, J. M. *J. Chem. Phys.* **1994**, *101*, 6233.
(4) Giordmaine, J. A. *Phys. Rev.* **1965**, *138*, A1599.
(5) Belkin, M. A.; Han, S. H.; Wei, X.; Shen, Y. R. *Phys. Rev. Lett.* **2001**, *87*, 113001.
(6) Fischer, P.; Beckwitt, K.; Wise, F. W.; Albrecht, A. C. *Chem. Phys. Lett.* **2002**, *352*, 463.
(7) Cameron, R.; Tabisz, G. C. *Mol. Phys.* **1997**, *90*, 159.
(8) Mesnil, H.; Hache, F. *Phys. Rev. Lett.* **2000**, *85*, 4257.
(9) Alexandre, M.; Lemercier, G.; Andraud, C.; Mesnil, H.; Schanne-Klein, M. C.; Hache, F. *Synth. Met.* **2002**, *127*, 135.
(10) Fischer, P.; Wiersma, D. S.; Righini, R.; Champagne, B.; Buckingham, A. D. *Phys. Rev. Lett.* **2000**, *85*, 4253.
(11) Champagne, B.; Fischer, P.; Buckingham, A. D. *Chem. Phys. Lett.* **2000**, *331*, 83.
(12) Belkin, M. A.; Kulakov, T. A.; Ernst, K.-H.; Yan, L.; Shen, Y. R. *Phys. Rev. Lett.* **2000**, *85*, 4474.
(13) Byers, J. D.; Hicks, J. M. *Chem. Phys. Lett.* **1994**, *231*, 216.
(14) Belkin, M. A.; Shen, Y. R.; Flytzanis, C. *Chem. Phys. Lett.* **2002**, *363*, 479.
(15) Hanazaki, I.; Akimoto, H. *J. Am. Chem. Soc.* **1972**, *94*, 4102.
(16) Boyd, R. W. *Nonlinear Optics*; Academic Press: Boston, 1992.
(17) Brueckner, K. A. *Phys. Rev.* **1955**, *100*, 35.
(18) Dunning, T. H. *J. Chem. Phys.* **1989**, *90*, 1007.
(19) Frisch, M. J.; et al.. *Gaussian 98*, Revision A.9; Gaussian Inc.: Pittsburgh, PA, 1998.
(20) Deussen, H.-J.; Hendrickx, E.; Boutton, C.; Krog, D.; Clays, K.; Bechgaard, K.; Persoons, A.; Bjornhølm, T. *J. Am. Chem. Soc.* **1996**, *118*, 6841.
(21) Fischer, P.; Buckingham, A. D.; Albrecht, A. C. *Phys. Rev. A* **2001**, *64*, 053816.
(22) Yang, P. K.; Huang, J. Y. *J. Opt. Soc. Am. B* **1998**, *15*, 1698.
(23) Quinet, Q.; Champagne B. *Int. J. Quantum Chem.* **2001**, *85*, 463.
(24) van Beek, J. B.; Kajzar, F.; Albrecht, A. C. *J. Chem. Phys.* **1991**, *95*, 6400.
(25) Champion, P. M.; Albrecht, A. C. *J. Chem. Phys.* **1980**, *72*, 6498.
(26) Mori, K.; Masuda, Y.; Kashino, S. *Acta Crystallogr., Sect. C* **1993**, *49*, 1224.
(27) Nakao, K.; Kyogoku, Y.; Sugeta, H. *Faraday Discuss.* **1994**, *99*, 77.
(28) Kanis, D. R.; Ratner, M. A.; Marks, T. J. *Chem. Rev.* **1994**, *94*, 195.
(29) Szymanski, H. A. *Interpreted Infrared Spectra*; Plenum Press: New York, 1964; Vols. 1−3.
(30) Nogueira, H. I. S.; Quintal, S. M. O. *Spectrochim. Acta A* **2000**, *56*, 959.
(31) Pershan, P. S. *Phys. Rev.* **1963**, *130*, 919.
(32) Jeffreys, H. *Cartesian Tensors*; CUP: Cambridge, 1974.
(33) Barron, L. D.; Buckingham, A. D. *Acc. Chem. Res.* **2001**, *34*, 781.
(34) Bethune, D. S.; Smith, R. W.; Shen, Y. R. *Phys. Rev. Lett.* **1976**, *37*, 431.
(35) The divisor of 2! in the expressions relating the hyperpolarizabilities to their susceptibilities is absent when derived by the time-ordered density matrix approach.
(36) Adler, E. *Phys. Rev.* **1964**, *134*, A728.
(37) Flytzanis, C. In *Quantum Electronics*; Rabin, H., Tang, C. L., Eds.; Academic: New York, 1975; Vol. 1, Part A.
(38) Wei, X.; Hong, S.-C.; Lvovsky, A. I.; Held, H.; Shen, Y. R. *J. Phys. Chem. B* **2000**, *104*, 3349.
(39) Kauranen, M.; Maki, J. J.; Verbiest, T.; van Elshocht, S.; Persoons, A. *Phys. Rev. B* **1997**, *55*, R1985.
(40) Schanne-Klein, M. C.; Hache, F.; Roy, A.; Flytzanis, C. *J. Chem. Phys.* **1998**, *108*, 9436.
(41) The first hyperpolarizability $\beta^{(eee)}$ has atomic units $e^3a_0^3E_h^{-2}$. Its conversion to the esu is given by 1 atomic unit = 8.641×10^{-33} cm^5 esu^{-1}, and to SI units by 1 atomic unit = 3.206×10^{-53} C m^3 V^{-2} (see ref 28).